2.5D MULTIZONE REPRODUCTION WITH ACTIVE CONTROL OF SCATTERED SOUND FIELDS

Junqing Zhang[1], Wen Zhang[1,2], Thushara D. Abhayapala[2], Jingli Xie[1] and Lijun Zhang[1]

[1]Center of Intelligent Acoustics and Immersive Communications
Northwestern Polytechnical University, Xi'an, Shaanxi 710072, China
[2]Research School of Engineering, College of Engineering and Computer Science
The Australian National University, Canberra, ACT 0200, Australia

ABSTRACT

Multizone reproduction has been focused on reproducing sounds in an empty listening space. However, there are always scatterers such as human heads in sound zones, generating scattered sound fields and causing degraded system performance. In this work, we develop a modal-domain method for 2.5D multizone reproduction with a solid object in the bright zone. Analytical expressions of the incident and scattered fields are developed. We then propose an active control strategy to correct the scattering effect. In the reproduction stage, we use the weighted mode matching approach to achieve the optimal control over the entire region. Simulation results show that in comparison with the conventional method which does not consider the scattering effect, the proposed method can achieve higher acoustic contrast performance over a broadband frequency range.

Index Terms— Multizone reproduction, 2.5D reproduction, mode matching, scatterer

1. INTRODUCTION

Multizone reproduction aims to reproduce sounds over multiple regions of space without physical isolation using a single loudspeaker array [1]. This arrangement allows sound zones to be produced at any desired location and also the listener to freely move within space. Thus, it can provide significant flexibility and has a wide range of audio applications, such as in car audio systems and creating quiet zones in shared environments [2, 3]. Many approaches have been developed, which can be broadly classified into four categories, acoustic contrast control (ACC) [4–9] , pressure matching (PM) [10–13] , the combination of ACC and PM [14–17] , and mode matching based reproduction [18–23]. In mode matching based reproduction, the theory is mainly developed for the 2D case. A practical implementation is known as 2.5D reproduction, that is to control 2D desired fields using 3D secondary sources [24, 25]. A weighted mode matching approach for 2.5D reproduction is developed to achieve optimal control within the global region [26].

Multizone reproduction has been focused on reproducing sounds in an empty listening space. In practice, the listener exists in these sound zones, resulting in scattered sound fields and deterioration of system performance. Experimental results further prove that the scattering effect from listeners causes around 8 dB acoustic contrast loss in multizone reproduction [27]. A modified ACC approach was developed based on modelling the scatterer in the bright zone as a rigid sphere, which can achieve around 1-4 dB gain in acoustic contrast for frequency above 1000Hz [28]. Based on the same assumption, the scattering effect has been investigated with corrected solutions proposed in mode matching based sound field reproduction [29, 30]. Recently, an active control strategy was developed to control the scattered sound field from a rigid sphere by optimizing the loudspeaker placement in the 3D reproduction system [31].

In this paper, we develop a modal-domain method for 2.5D multizone reproduction with a solid object in the bright zone, which was not considered in the previous work. The object, for example the human head, is modelled as a rigid sphere. Analytical expressions of the incident and scattered fields are developed for the global region and each sound zone. We then propose an active control strategy to correct the scattering effect. In the reproduction stage, we use the weighted mode matching approach to achieve the optimal control over the entire region. The effectiveness of the proposed method is demonstrated through simulation-based experiments.

2. MULTIZONE REPRODUCTION

In this work, we control sound fields in multiple non-overlapping regions, on a 2D plane with an assumption that there is a scatterer of human head in the bright zone as shown in Fig. 1. Each sound zone q has a radius r_q and its center is denoted by $\boldsymbol{O}_q$ with respect to the global origin $\boldsymbol{O}$, i.e., the bright zone and dark zone. Any observation point in a sound zone is represented by $\boldsymbol{x}_q$ with respect to $\boldsymbol{O}_q$, or $\boldsymbol{x} = \boldsymbol{x}_q + \boldsymbol{O}_q$ with respect to $\boldsymbol{O}$.

2.1. Soundfield model

The soundfield at any point $\boldsymbol{x}$ consists of two parts, i.e. the incident field and the field caused by scattering from human head,

$$P(\boldsymbol{x}, k) = P^{\text{in}}(\boldsymbol{x}, k) + P^{\text{sc}}(\boldsymbol{x}, k). \tag{1}$$

where superscript in and sc denote incident field and scattered field, respectively. In the following, we will derive modal-domain representation of each part and the corresponding relationship between the global region and local zones.

2.1.1. *Incident sound field*

A 3D source-free incoming field at an arbitrary point $\boldsymbol{x} = (\|\boldsymbol{x}\|, \theta, \phi)$ can be approximately represented in terms of a harmonic decomposition of the form

$$P^{\text{in}}(\boldsymbol{x}, k) \approx \sum_{n=0}^{N_0} \sum_{m=-n}^{n} \beta_{nm}^{\text{in}}(k) j_n(k\|\boldsymbol{x}\|) Y_n^m(\theta, \phi), \tag{2}$$

e-mail: junqingzhang@mail.nwpu.edu.cn

This work was supported by the National Natural Science Foundation of China (NSFC) funding scheme under Project No. 61671380.

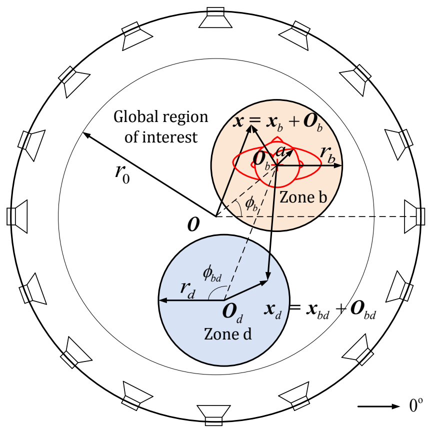

Fig. 1. Geometry of multizone sound control with a human head inside the bright zone.

where $k = 2\pi f/c$ is the wave number with f being the frequency and c the speed of sound, $j_n(\cdot)$ is the spherical Bessel function of order n, and Y_n^m denotes the spherical harmonics of order n and degree m. $\beta_{nm}(k)$ is the decomposition coefficient and the truncation order $N_0 = \lceil ekr_0/2 \rceil$ [32], where r_0 is the radius of the region of interest, e is the Euler's number, and $\lceil \cdot \rceil$ denotes the ceiling function.

For 2.5D reproduction, the desired field is on a 2D plane. Thus, by setting the elevation angle $\theta = \pi/2$, the sound pressure can be written as,

$$P^{\text{in}}(\boldsymbol{x}, k) \approx \sum_{m=-N_0}^{N_0} \sum_{n=|m|}^{N_0} \beta_{nm}^{\text{in}}(k) j_n(k \|\boldsymbol{x}\|) Y_n^m e^{im\phi_{\boldsymbol{x}}}, \tag{3}$$

where $Y_n^m(\frac{\pi}{2}, \phi_{\boldsymbol{x}}) = Y_n^m e^{im\phi_{\boldsymbol{x}}}$, with $Y_n^m = C_n^m P_n^m(0)$ and $C_n^m = \sqrt{\frac{2n+1}{4\pi} \frac{(n-|m|)!}{(n+|m|)!}}$. Analogous to (3), the incident sound field at any observation point $\boldsymbol{x}_b \equiv (\|\boldsymbol{x}_b\|, \phi_{\boldsymbol{x}_b})$ within the bright zone can be expressed in the form

$$P_b^{\text{in}}(\boldsymbol{x}_b, k) \approx \sum_{\mu=-N_b}^{N_b} \sum_{\nu=|\mu|}^{N_b} \alpha_{\nu\mu}^{\text{in}}(k) j_\nu(k \|\boldsymbol{x}_b\|) Y_\nu^\mu e^{i\mu\phi_{\boldsymbol{x}_b}}, \tag{4}$$

where $\alpha_{\nu\mu}^{\text{in}}$ is the corresponding soundfield coefficients and the truncation order is $N_b = \lceil ekr_b/2 \rceil$.

The bright zone soundfield coefficients $\alpha_{\nu\mu}^{\text{in}}$ in (4) can be related to the global soundfield coefficients β_{nm}^{in} in (3) using the spherical Bessel function addition theorem [33], that is

$$\sum_{m=-N_0}^{N_0} \sum_{n=|m|}^{N_0} \beta_{nm}^{\text{in}}(k) T_{n\nu}^{m\mu}(\boldsymbol{O}_b, k) = \alpha_{\nu\mu}^{\text{in}}(k), \tag{5}$$

where

$$T_{n\nu}^{m\mu}(\boldsymbol{O}_b, k) = 4\pi i^{\nu-n} W_1 W_2 \sum_{\ell=0}^{\infty} i^l (-1)^{2m-\mu} j_\ell(k \|\boldsymbol{O}_b\|) \times \overline{Y_{\ell(\mu-m)}}(\theta_{\boldsymbol{O}_b}, \phi_{\boldsymbol{O}_b}) \sqrt{\frac{(2n+1)(2\nu+1)(2\ell+1)}{4\pi}}, \tag{6}$$

W_1 and W_2 denote the Wigner $3-j$ symbol, and $\overline{(\cdot)}$ represents the complex conjugate.

Using the matrix-vector notation, we can represent (5) as

$$\boldsymbol{T}_{\text{b}} \boldsymbol{b}^{\text{in}} = \boldsymbol{a}_{\text{b}}^{\text{in}}. \tag{7}$$

where $\boldsymbol{b}^{\text{in}} = [\beta_0^{\text{in}}, \ldots, \beta_{n^2+n+m+1}^{\text{in}}, \ldots, \beta_{(N_0+1)^2}^{\text{in}}]^T$, $\boldsymbol{a}_{\text{b}}^{\text{in}} = [\alpha_0^{\text{in}}, \ldots, \alpha_{1+\nu^2+\nu+\mu}^{\text{in}}, \ldots, \alpha_{(N_b+1)^2}^{\text{in}}]^T$, and $\boldsymbol{T}_{\text{b}}$ is the $(N_b+1)^2 \times (N_0+1)^2$ translation matrix. Similarly, we can use the matrix $\boldsymbol{T}_{\text{d}}$ to denote translation from the global region to the dark zone.

2.1.2. *Scattered sound field*

We model the human head as a rigid sphere, which can produce an outgoing scattered wave when the incident wave hits on it. By applying the boundary condition on its surface, that is the particle velocity perpendicular to the surface is zero [34], we can derive the analytical expression of the scattered field within the bright zone,

$$P_b^{\text{sc}}(\boldsymbol{x}_b, k) \approx \sum_{\mu=-N_h}^{N_h} \sum_{\nu=|\mu|}^{N_h} \alpha_{\nu\mu}^{\text{sc}} h_\nu^{(1)}(k \|\boldsymbol{x}_b\|) Y_\nu^\mu e^{i\mu\phi_{\boldsymbol{x}_b}}, \tag{8}$$

where $h_\nu^{(1)}(\cdot)$ represents the outing spherical Hankel functions,

$$\alpha_{\nu\mu}^{\text{sc}} = -\frac{j_\nu'(ka)}{h_\nu^{(1)'}(ka)} \alpha_{\nu\mu}^{\text{in}}, \tag{9}$$

and $(\cdot)'$ denotes the corresponding derivative. The truncation order is $N_h = \lceil eka/2 \rceil$ with a the radius of the human head.

We are particularly interested in the scattered field within the dark zone, which can be represented as

$$P_d^{\text{sc}}(\boldsymbol{x}_d, k) \approx \sum_{u=-N_d}^{N_d} \sum_{v=|v|}^{N_d} \zeta_{vu}^{\text{sc}} j_v(k \|\boldsymbol{x}_d\|) Y_v^u e^{iu\phi_{\boldsymbol{x}_d}}, \tag{10}$$

where $N_d = \lceil ekr_d/2 \rceil$ and r_d is the radius of the dark zone.

Analogous to (5), based on the corresponding addition theorem for $h_\mu^{(1)}(k \|\boldsymbol{x}_b\|) Y_\nu^\mu(\theta_{\boldsymbol{x}_b}, \phi_{\boldsymbol{x}_b})$ [33], we have

$$\sum_{\mu=-N_h}^{N_h} \sum_{\nu=|u|}^{N_h} \alpha_{\nu\mu}^{\text{sc}} S_{\nu v}^{\mu u}(\boldsymbol{O}_{bd}, k) = \zeta_{vu}^{\text{sc}}, \tag{11}$$

where

$$S_{\nu v}^{\mu u}(\boldsymbol{O}_{bd}, k) = 4\pi i^{v-\nu} W_3 W_4 \sum_{\ell=0}^{\infty} i^l (-1)^{2\mu-u} h_\ell(k \|\boldsymbol{O}_{bd}\|) \times \overline{Y_{\ell(u-\mu)}}(\theta_{\boldsymbol{O}_{bd}}, \phi_{\boldsymbol{O}_{bd}}) \sqrt{\frac{(2\nu+1)(2v+1)(2\ell+1)}{4\pi}}, \tag{12}$$

the vector $\boldsymbol{O}_{bd} = \boldsymbol{O}_b - \boldsymbol{O}_d$, W_3 and W_4 denote Wigner $3-j$ symbol.

The matrix-vector notation of (11) is

$$\boldsymbol{S}_{\text{bd}} \boldsymbol{a}_{\text{b}}^{\text{sc}} = \boldsymbol{c}_{\text{d}}^{\text{sc}}. \tag{13}$$

where $\boldsymbol{a}_{\text{b}}^{\text{sc}} = [\alpha_0^{\text{sc}}, \ldots, \alpha_{\nu^2+\nu+\mu+1}^{\text{sc}}, \ldots, \alpha_{(N_h+1)^2}^{\text{sc}}]^T$, $\boldsymbol{c}_d^{\text{sc}} = [\zeta_0^{\text{sc}}, \ldots, \zeta_{v^2+v+u+1}^{\text{sc}} \ldots, \zeta_{(N_d+1)^2}^{\text{sc}}]^T$, and $\boldsymbol{S}_{\text{bd}}$ is the $(N_d+1)^2 \times (N_h+1)^2$ translation matric.

2.2. Modified formulation and control

In the original formulation, the multizone reproduction problem in the modal domain is formulated as finding the global sound field coefficients $\boldsymbol{b}$ to generate a desired sound field in the bright zone characterised by its local coefficients $\boldsymbol{a}_{\mathrm{b}}^{\mathrm{in}}$ with constraints on the sound energy in the dark zone and the energy of the entire global sound field [26]. In the modified formulation, we aim to minimize the energy of both the incident and scattered sound fields in the dark zone. That is

$$\min_{\boldsymbol{b}} \quad \|\boldsymbol{T}_{\mathrm{b}}\boldsymbol{b} - \boldsymbol{a}_{\mathrm{b}}^{\mathrm{in}}\|^2 \tag{14}$$

$$\text{subject to} \quad \|(\boldsymbol{T}_{\mathrm{d}} + \boldsymbol{R}_{\mathrm{d}})\boldsymbol{b}\|^2 \leq e_{\mathrm{d}} \tag{14a}$$

$$\|\boldsymbol{b}\|^2 \leq e_{\mathrm{g}}, \tag{14c}$$

where based on (9) and (13), the scattering components are linked to the incident sound fields and also the global components, that is

$$\boldsymbol{c}_{\mathrm{d}}^{\mathrm{sc}} = \boldsymbol{R}_{\mathrm{d}}\boldsymbol{b}, \quad \boldsymbol{R}_{\mathrm{d}} = \boldsymbol{S}_{\mathrm{bd}}\boldsymbol{Q}\boldsymbol{E}\boldsymbol{T}_{\mathrm{b}}. \tag{15}$$

The matrix $\boldsymbol{Q} = \mathrm{diag}\big(-j_0^{'}(ka)/h_0^{(1)'}(ka)\ldots -j_{N_h}^{'}(ka)/h_{N_h}^{(1)'}(ka)\big)$ is a diagonal matrix and the matrix $\boldsymbol{E}$ is used to pick the first $(N_h+1)^2$ elements of the vector $\boldsymbol{a}_{\mathrm{b}}^{\mathrm{in}}$ given the truncation order of the scattered field in the bright zone is N_h.

We can then use the method of Lagrange multipliers to obtain the global desired sound field coefficients,

$$\boldsymbol{b} = [\overline{\boldsymbol{T}_{\mathrm{b}}}\boldsymbol{T}_{\mathrm{b}} + \lambda_1\overline{(\boldsymbol{T}_{\mathrm{d}}+\boldsymbol{R}_{\mathrm{d}})}(\boldsymbol{T}_{\mathrm{d}}+\boldsymbol{R}_{\mathrm{d}}) + \lambda_2\boldsymbol{I}]^{-1}\overline{\boldsymbol{T}}_{\mathrm{b}}\boldsymbol{a}_{\mathrm{b}}^{\mathrm{in}}. \tag{16}$$

where λ_1 and λ_2 are positive Lagrange multipliers.

3. 2.5D WEIGHTED MODE MATCHING REPRODUCTION

An array of L loudspeakers is used for reproduction and its generated global sound field can be written as

$$P(\boldsymbol{x},k) = \sum_{\ell=1}^{L} d_\ell(k) G_\ell(\boldsymbol{x},k), \tag{17}$$

where $G_\ell(\boldsymbol{x},k)$ represents the acoustic transfer function (ATF) between the ℓth loudspeaker and the observation point $\boldsymbol{x}$ in the global system and d_ℓ is the loudspeaker weight.

The ATF is parameterised in the modal domain as

$$G_\ell(\boldsymbol{x},k) \approx \sum_{m=-N_0}^{N_0}\sum_{n=|m|}^{N_0} \gamma_n^m(\ell,k) j_n(k\|\boldsymbol{x}\|) Y_n^m e^{im\phi_{\boldsymbol{x}}}, \tag{18}$$

where $\gamma_n^m(\ell,k)$ are ATF coefficients for the ℓth speaker. Note that each loudspeaker is a 3D point source, there are $(N_0+1)^2$ coefficients to describe its ATF within the global control region. The ATF coefficients are assumed to be a prior knowledge obtained from theoretical solutions or pre-calibration [35]. In anechoic condition $\gamma_n^m(\ell,k) = -ikh_n^{(2)}(kr_\ell)\overline{Y_n^m(\pi/2,\phi_\ell)}$.

Then, the generated 3D sound field is

$$P(\boldsymbol{x},k) \approx \sum_{m=-N_0}^{N_0}\sum_{\ell=1}^{L} d_\ell(k) \sum_{n=|m|}^{N_0} \gamma_n^m(\ell,k) j_n(k\|\boldsymbol{x}\|) Y_n^m e^{im\phi_{\boldsymbol{x}}}. \tag{19}$$

Note that the desired field given in (2) is 2D, or height-invariant, which needs to be controlled within a global region including multiple sound zones. We adopt the weighted mode matching approach for the optimal control [26]. That is, by referring to (3), the cost function is

$$\mathcal{J}(d,k) = \frac{1}{2\pi}\int_D \Big|P(\boldsymbol{x},k) - P^{\mathrm{in}}(\boldsymbol{x},k)\Big|^2 d\boldsymbol{x}. \tag{20}$$

Writing (20) in matrix form, we have

$$\mathcal{J}(d,k) = \boldsymbol{d}^H\boldsymbol{\mathcal{H}}\boldsymbol{d} - \boldsymbol{\mathcal{B}}^H\boldsymbol{d} - \boldsymbol{d}^H\boldsymbol{\mathcal{B}} + C. \tag{21}$$

with

$$[\boldsymbol{\mathcal{H}}]_{\ell 1,\ell 2} = \sum_{m=-N_0}^{N_0}\sum_{n=|m|}^{N_0}\sum_{n'=|m|}^{N_0} \omega_{n,n'}^m \overline{\gamma_n^m(\ell_1,k)}\gamma_{n'}^m(\ell_2,k)$$

$$[\boldsymbol{\mathcal{B}}]_{\ell 1} = \sum_{m=-N_0}^{N_0}\sum_{n=|m|}^{N_0}\sum_{n'=|m|}^{N_0} \omega_{n,n'}^m \overline{\gamma_n^m(\ell_1,k)}\beta_{mn'}^{\mathrm{in}}(k) \tag{22}$$

where

$$\omega_{n,n'}^m \equiv Y_n^m Y_{n'}^m \int_0^{r_0} j_n(kr) j_{n'}(kr) r dr \tag{23}$$

We write

$$\boldsymbol{\mathcal{H}} = \boldsymbol{\Gamma}^H\boldsymbol{W}\boldsymbol{\Gamma}, \tag{24}$$

where the ATF coefficient matrix $\boldsymbol{\Gamma}$ is defined as $[\boldsymbol{\Gamma}]_{n^2+n+m+1,\ell} = \gamma_n^m(\ell,k)$ and $\boldsymbol{W}$ is a $(N_0+1)^2$-square weighting matrix defined as

$$[\boldsymbol{W}]_{n^2+n+m+1,n'^2+n'+m'+1} = \delta_{m-m'} w_{n,n'}^m \tag{25}$$

Similarly, it can be defined that

$$\boldsymbol{\mathcal{B}} = \boldsymbol{\Gamma}^H\boldsymbol{W}\boldsymbol{b}, \tag{26}$$

where $[\boldsymbol{b}]_{n^2+n+m+1} = \beta_{mn}^{\mathrm{in}}(k)$.

Minimizing $\mathcal{J}$ in (21), the solution is

$$\widehat{\boldsymbol{d}} = \boldsymbol{\mathcal{H}}^{-1}\boldsymbol{\mathcal{B}} = (\boldsymbol{\Gamma}^H\boldsymbol{W}\boldsymbol{\Gamma})^{-1}\boldsymbol{\Gamma}^H\boldsymbol{W}\boldsymbol{b}. \tag{27}$$

4. EVALUATION

4.1. Simulation setup

We simulate two-zone reproduction examples in anechoic chamber. The radius of the global control region is $r_0 = 1.4$m. The virtual source, which is located in the far field and incident from $\phi_V = 2\pi/3$, produce a monochromatic 3D plane wave of frequency 1400 Hz. The bright zone and dark zone are located at $\mathbf{O}_b = (0.4, 0)$ and $\mathbf{O}_d = (-0.4, 0)$ with respect to the global origin, respectively. Each sound zone has a radius of 0.25m. A scatterer of a rigid sphere is located at the center of the bright zone and its radius is set to 0.1m, i.e., approximately the human head size. A 99-element circular loudspeaker array of radius 2 m is used for reproduction. The Newtons method [21] is used to solve the Lagrange multipliers λ_1 and λ_2 in (16). We set the energy constraints in the dark zone and global region to $e_d = 0$dB and $e_g = 20$dB, respectively.

The performance measures are the acoustic contrast $\kappa(k)$ between the bright zone and dark zone, and the bright zone reproduction error $\varepsilon(k)$, i.e.,

$$\kappa(k) = 10\log_{10}\frac{\frac{1}{\mathbb{V}_b}\int_{\mathbb{D}_b}\Big|P(\boldsymbol{x},k)\Big|^2 d\boldsymbol{x}}{\frac{1}{\mathbb{V}_d}\int_{\mathbb{D}_d}\Big|P(\boldsymbol{x},k)\Big|^2 d\boldsymbol{x}} \tag{28}$$

$$\varepsilon(k) = 10\log_{10}\frac{\frac{1}{\mathbb{V}_b}\int_{\mathbb{D}_b}\Big|P(\boldsymbol{x},k) - P_d(\boldsymbol{x},k)\Big|^2 d\boldsymbol{x}}{\frac{1}{\mathbb{V}_b}\int_{\mathbb{D}_b}\Big|P(\boldsymbol{x},k)\Big|^2 d\boldsymbol{x}}, \tag{29}$$

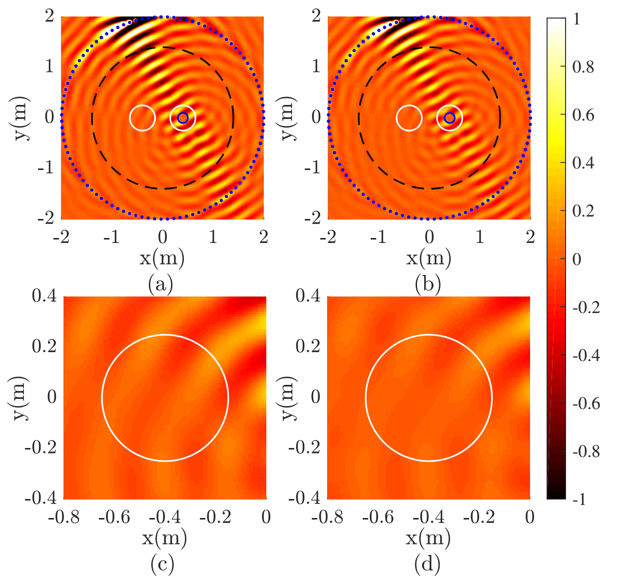

Fig. 2. Examples of 2.5D multizone reproduction with a scatterer at the bright zone center denoted by the blue solid circle. Results are shown for (a) the method without controlling the scattering effect [26] and (b) the proposed method with active control of the scattered sound field. The corresponding scale-up results in the dark zone are shown in (c) and (d). Blue · marks denote the locations of loudspeakers.The area in the black dashed line and white solid line correspond to the global region, bright zone and dark zone, respectively.

where $P(\boldsymbol{x}, k)$ and $P_d(\boldsymbol{x}, k)$ represent the reproduced sound field and the desired sound field at a point within the bright zone $\mathbb{D}_b$ or the dark zone $\mathbb{D}_d$. $\mathbb{V}_b$ and $\mathbb{V}_d$ denote the area of the bright zone and the dark zone, respectively.

4.2. Simulation Results

The real part of the reproduced results are plotted in Fig.2. The display is limited to the maximum value of the reconstructed field within the bright zone. As shown in Fig. 2 (a), using the traditional method without considering the scattering effect [26], the sound field scattered by the rigid sphere will enter the dark zone. The wavefront within the bright zone also distorts. Especially, the effect of the scatterer is considerable when the bright zone and dark zone are close. Compering the results in (c) and (d), we can see that using the proposed method with active control of the scattered sound field, the sound level in the dark zone can be effectively reduced.

We further evaluate the system performance over a broadband frequency range of $[0.1, 2]$ kHz. The reproduction setup is the same as in the example of Fig. 2. The blue, black and red lines correspond to the case that there is no scatterer (Incident), using the traditional method without scattering control (Scattered) [26], and using the proposed scattering control method (Proposed). The driving signals for the first two cases are the same. The results in Fig. 3(a) shows that the acoustic contrast has $0.5-4$ dB loss when the scatterer is in the bright zone. Using the proposed method, about $1.5-4$ dB gain in acoustic contrast is achieved in the frequency range of $[0.3, 2]$ kHz. In Fig. 3.(b), these three methods show roughly the same bright zone reproduction error performance.

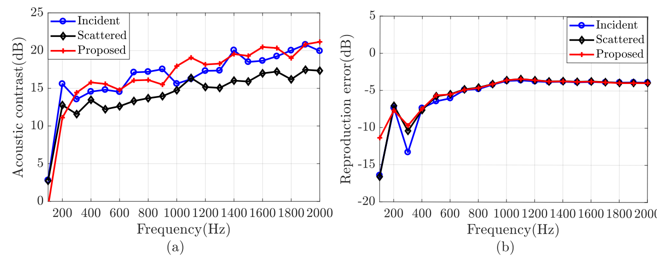

Fig. 3. Plots show (a) acoustic contrast and (b) bright zone reproduction error over a broadband frequency range.

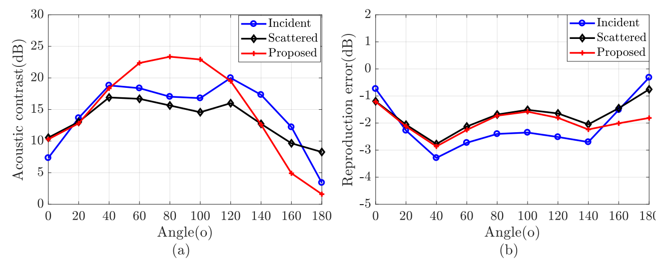

Fig. 4. Plots show (a) acoustic contrast and (b) bright zone reproduction error over 180° angle range.

Finally, we compare the performance of these three methods over a 180° angle range. As shown in Fig. 4 (a), for the plane wave coming from 20° to 160°, its incidence on the scatterer produces considerable effects into the dark zone with around 2-5 dB loss of the acoustic contrast. The proposed method is quite effective for this angle range, and the biggest improvement is nearly 8 dB at the direction of 100° incidence. However, the proposed method does not improve the acoustic contrast within the angle range of 140° to 180°. This is analogous to the occlusion problem with a large amount of scattered waves going into the dark zone. For this angle range, adding additional constraints also causes the bright zone reproduction error to increase.

5. CONCLUSION

A modal-domain approach to 2.5D multizone reproduction with active control of scattered sound fields was presented. The scatterer, i.e., the human head, was modelled as a rigid sphere located at the bright zone center. Based on wave modelling theory and translation theorem, we developed analytical expressions of the incident and scattered fields for the global region and each sound zone. We then proposed an active control strategy to correct the scattering effect and used the weighted mode matching approach for reproduction. Simulation results showed that the proposed method can achieve higher acoustic contrast performance over a wide frequency range. Future work will extend the method to reverberant environment with experimental validation.

6. REFERENCES

[1] T. Betlehem, W. Zhang, M. A. Poletti, and T. D. Abhayapala, "Personal sound zones: Delivering interface-free audio to multiple listeners," *IEEE Signal Process. Mag.*, vol. 32, no. 2, pp. 81–91, 2015.

[2] J. Cheer, S. J. Elliott, and M. F. S. Gálvez, "Design and implementation of a car cabin personal audio system," *J. Acoust. Soc. Am.*, vol. 61, no. 6, pp. 414–424, 2013.

[3] T. Abhayapala and Y. Wu, "Spatial soundfield reproduction with zones of quiet," in *Audio Eng. Soc. (AES) Conv.*, (New York, USA), p. 7 pages, Oct. 2009.

[4] J.-W. Choi and Y.-H. Kim, "Generation of an acoustically bright zone with an illuminated region using multiple sources," *J. Acoust. Soc. Am.*, vol. 111, no. 4, pp. 1695–1700, 2002.

[5] M. Shin, S. Q. Lee, F. M. Fazi, P. A. Nelson, D. Kim, S. Wang, K. H. Park, and J. Seo, "Maximization of acoustic energy difference between two spaces," *J. Acoust. Soc. Am.*, vol. 128, pp. 121–131, 2010.

[6] S. J. Elliott, J. Cheer, J.-W. Choi, and Y.-H. Kim, "Robustness and regularization of personal audio systems," *IEEE Trans. Audio, Speech, Lang. Process.*, vol. 20, no. 7, pp. 2123–2133, 2012.

[7] P. Coleman, P. Jackson, M. Olik, and J. A. Pederson, "Personal audio with a planar 432 bright zone," *J. Acoust. Soc. Am.*, vol. 136, no. 4, pp. 1725–1735, 2014.

[8] P. Coleman, P. Jackson, M. Olik, M. Mller, M. Olsen, and J. A. Pederson, "Acoustic contrast, planarity and robustness of sound zone methods using a circular loudspeaker array," *J. Acoust. Soc. Am.*, vol. 135, no. 4, pp. 1929–1940, 2014.

[9] Y. Cai, M. Wu, L. Liu, and J. Yang, "Time-domain acoustic contrast control design with response differential constraint in personal audio systems," *J. Acoust. Soc. Am.*, vol. 135, no. 6, pp. 252–257, 2014.

[10] M. A. Poletti, "An investigation of 2D multizone surround sound systems," in *Audio Eng. Soc. (AES) Conv.*, (San Francisco, USA), p. 9 pages, Oct. 2008.

[11] T. Betlehem and C. Withers, "Sound field reproduction with energy constraint on loudspeaker weights," *IEEE Trans. Audio, Speech, Lang. Process.*, vol. 20, no. 8, pp. 2388–2392, 2012.

[12] N. Radmanesh and I. S. Burnett, "Generation of isolated wideband sound field using a combined two-stage Lasso-LS algorithm," *IEEE Trans. Audio, Speech, Lang. Process.*, vol. 21, no. 2, pp. 378–387, 2013.

[13] W. Jin and W. B. Kleijn, "Multizone sound field reproduction in reverberant rooms using compressed sensing techniques," in *Proc. IEEE ICASSP*, (Florence, Italy), pp. 4728–4732, May 2014.

[14] J.-H. Chang and F. Jacobsen, "Sound field control with a circular double-layer array of loudspeakers," *J. Acoust. Soc. Am.*, vol. 131, no. 6, pp. 4518–4525, 2012.

[15] J.-H. Chang and F. Jacobsen, "Experimental validation of sound field control with a circular double-layer array of loudspeakers," *J. Acoust. Soc. Am.*, vol. 133, pp. 2046–2054, 2013.

[16] W. Jin, W. B. Kleijn, and D. Virette, "Multizone soundfield reproduction using orthogonal basis expansion," in *Proc. IEEE ICASSP*, (Vancouver, Canada), pp. 311–315, May 2013.

[17] S. Galvez, F. Marcos, S. J. Elliott, and C. Jordan, "Time domain optimisation of filters used in a loudspeaker array for personal audio," *IEEE Trans. Audio, Speech, Lang. Process.*, vol. 13, no. 11, pp. 1869–1878, 2015.

[18] Y. Wu and T. D. Abhayapala, "Spatial multizone soundfield reproduction: Theory and design," *IEEE Trans. Audio, Speech, Lang. Process.*, vol. 19, pp. 1711–1720, June 2011.

[19] W. Jin and W. B. Kleijn, "Theory and design of multizone soundfield reproduction using sparse methods," *IEEE Trans. Audio, Speech, Lang. Process.*, vol. 23, no. 12, pp. 2343 – 2355, 2015.

[20] M. A. Poletti and F. M. Fazi, "An approach to generating two zones of silence with application to personal sound systems," *J. Acoust. Soc. Am.*, vol. 137, no. 2, pp. 598–605, 2015.

[21] W. Zhang, T. D. Abhayapala, T. Betlehem, and F. M. Fazi, "Analysis and control of multi-zone sound field reproduction using modal-domain approach," *J. Acoust. Soc. Am.*, vol. 140, pp. 2134–2144, 2016.

[22] J. Donley, C. Ritz, and W. B. Kleijn, "Multizone soundfield reproduction with privacy-and quality-based speech masking filters," *IEEE Trans. Audio, Speech, Lang. Process.*, vol. 26, no. 6, pp. 1041–1055, 2018.

[23] Z. Han, M. Wu, Q. Zhu, and J. Yang, "Two-dimensional multizone sound field reproduction using a wave-domain method," *J. Acoust. Soc. Am.*, vol. 144, no. 3, pp. 185–190, 2018.

[24] F. Winter, J. Ahrens, and S. Spors, "On analytic methods for 2.5-D local sound field synthesis using circular distributions of secondary sources," *IEEE Trans. Audio, Speech, Lang. Process.*, pp. 914–926, May 2016.

[25] T. Okamoto, "Analytical approach to 2.5d sound field control using a circular double-layer array of fixed-directivity loudspeakers," in *Proc. IEEE ICASSP*, (New Orleans, USA), pp. 91–95, March 2017.

[26] W. Zhang, J. Zhang, T. D. Abhayapala, and L. Zhang, "2.5 D multizone reproduction using weighted mode matching," in *Proc. IEEE ICASSP*, (Calgary, Alberta, Canada), pp. 476–480, IEEE, 2018.

[27] M. Olsen and M. B. Møller, "Sound zones: Scattering study with head and torso simulator," in *Audio Eng. Soc. (AES) Conv.*, (Guildford, USA), p. 9 pages, Sep. 2013.

[28] J.-H. Chang, J.-Y. Park, and Y.-H. Kim, "Scattering effect on the sound focused personal audio system," *J. Acoust. Soc. Am.*, vol. 125, no. 5, pp. 3060–3066, 2009.

[29] T. Betlehem and M. A. Poletti, "Sound field reproduction around a scatterer in reverberation," in *Proc. IEEE ICASSP*, (Taipei, China), pp. 89–92, IEEE, 2009.

[30] J. Ahrens and S. Spors, "On the scattering of synthetic sound fields," in *Audio Eng. Soc. (AES) Conv.*, (London, UK), p. 7 pages, May 2011.

[31] J. Liu, X. Wang, M. Wu, and J. Yang, "An active control strategy for the scattered sound field control of a rigid sphere," *J. Acoust. Soc. Am.*, vol. 144, no. 1, pp. 52–58, 2018.

[32] R. A. Kennedy, P. Sadeghi, T. D. Abhayapala, and H. M. Jones, "Intrinsic limits of dimensionality and richness in random multipath fields," *IEEE Transa. Signal Process.*, vol. 55, pp. 2542–2556, June 2007.

[33] P. A. Martin, *Multiple scattering: interaction of time-harmonic waves with N obstacles*. No. 107, Cambridge University Press, pp.87-90, 2006.

[34] E. G. Williams, *Fourier Acoustics: Sound Radiation and Nearfield Acoustical Holography*. San Diego, CA: Academic Press, pp. 334-232, 1999.

[35] T. Betlehem and T. D. Abhayapala, "Theory and design of sound field reproduction in reverberant rooms," *J. Acoust. Soc. Am.*, vol. 117, no. 4, pp. 2100–2111, 2005.